Revision 1

A first-principles study of water in wadsleyite and ringwoodite: Implication for the 520-km discontinuity

Wenzhong Wang[a, b, c, *], Zhongqing Wu[a, d, e]

[a]Laboratory of Seismology and Physics of Earth's Interior, School of Earth and Space Sciences, University of Science and Technology of China, Hefei, Anhui 230026, China

[b]Department of Earth Sciences, University College London, London WC1E 6BT, United Kingdom

[c]Earth and Planets Laboratory, Carnegie Institution for Science, Washington, DC 20015, USA

[d]National Geophysical Observatory at Mengcheng, University of Science and Technology of China, Hefei, China

[e]CAS Center for Excellence in Comparative Planetology, USTC, Hefei, Anhui 230026, China

*Correspondence to: Wenzhong Wang (wz30304@mail.ustc.edu.cn or wenzhong.wang@ucl.ac.uk)

Abstract

The seismic discontinuity around 520 km is believed to be caused by the phase transition from wadsleyite to ringwoodite, the dominant minerals in the mantle transition zone (MTZ). Both wadsleyite and ringwoodite can contain more than one weight percentage of water at MTZ's conditions, but it is not well known how water affects the wadsleyite-ringwoodite transition. Here we investigated water partitioning between wadsleyite and ringwoodite and the water effect on this phase boundary using first-principles calculations. Our results show that the presence of water will shift the phase boundary to higher pressures and the width of the two-phase coexistence domain in the Mg_2SiO_4-H_2O system is insignificant at mid-MTZ conditions. For the $(Mg_{0.9}Fe_{0.1})_2SiO_4$ system, the incorporation of 1.0 wt% water can narrow the effective width of two-phase coexistence by two-thirds. Together with elastic data, we find that that velocity and impedance contrasts are only mildly changed by the water partitioning. We suggest that compared to the anhydrous condition, the presence of 1.0 wt% water will increase velocity gradients across the wadsleyite-ringwoodite transition by threefold, enhancing the detectability of the 520-km discontinuity.

Keywords: water partitioning, wadsleyite, ringwoodite, 520-km discontinuity, two-phase coexistence, mantle transition zone

1. Introduction

Seismological studies have provided some of the most direct observations on the Earth's mantle (Dziewonski and Anderson 1981; Kennett et al. 1995; Shearer and Flanagan 1999) and understanding its physical and chemical properties requires detailed knowledge from mineral physics. Olivine is the most abundant mineral in the Earth’s upper mantle and its volume percentage is ~60% in the widely accepted pyrolitic mantle composition (Ringwood 1962; Zou et al. 2018; Duan et al. 2019). The 410-km and 660-km discontinuities, which separate the upper mantle from the lower mantle, caused by the olivine-wadsleyite and post-spinel phase

transitions (Bina and Helffrich 1994; Helffrich and Wood 2001; Higo et al. 2001; Hirose 2002; Fei et al. 2004; Katsura et al. 2004), respectively. In the mid mantle transition zone (MTZ), wadsleyite is expected to undergo a phase transition to ringwoodite (Akaogi et al. 1989; Katsura and Ito 1989; Inoue et al. 2006; Yu et al. 2008; Tsujino et al. 2019), and some seismic studies have observed a seismic discontinuity around 520 km depth in some regions such as Northeastern China and central Asia (Shearer 1990; Gossler and Kind 1996; Deuss and Woodhouse 2001; Tian et al. 2016). However, unlike the 410-km and 660-km discontinuities, the 520-km discontinuity is not ubiquitously observed and absent in other regions such as the northeastern Pacific Ocean (Gossler and Kind 1996; Deuss and Woodhouse 2001). In particular, seismic studies have found two discontinuities at ~500 km and 560 km depths in some local regions (Deuss and Woodhouse 2001), rather than a single 520-km discontinuity. Therefore, understanding the nature of the wadsleyite-ringwoodite phase transition is of great importance for the interpretation of the 520-km discontinuity.

Many experimental studies have investigated the phase boundary between wadsleyite and ringwoodite and found that for the $(Mg_{0.9}Fe_{0.1})_2SiO_4$ system under dry condition, this phase transition occurs at ~520 km along the mantle adiabat, with a Clapeyron slope of ~+4.2 MPa/K (Akaogi et al. 1989; Katsura and Ito 1989; Inoue et al. 2006; Tsujino et al. 2019). The effective width of the two-phase coexistence is 20–22 km, which is much thicker than that of the olivine-wadsleyite binary loop (Inoue et al. 2006; Tsujino et al. 2019). The velocity and density contrasts (ΔV_P, ΔV_S, and $\Delta\rho$) between ringwoodite and wadsleyite are ~3.6%, 4.3%, and 1.9% (Núñez Valdez et al. 2012), respectively, smaller than those across the olivine-wadsleyite transition (Núñez-Valdez et al. 2013; Wang et al. 2019). In a pyrolitic composition consisting of ~60% wadsleyite, this phase transition can only result in a ΔV_P of ~2.1%, ΔV_S of 2.6%, and $\Delta\rho$ of 1.1% in a width of 20-22 km, probably making it difficult to be detected as a seismic discontinuity. However, it is not well known why the 520-km discontinuity could be observed in some local regions.

One of the most novel features of wadsleyite and ringwoodite is that they can store up to one weight percent of water at MTZ's conditions (Demouchy 2005; Jacobsen et al. 2005; Ohtani 2015; Fei and Katsura 2020), making the MTZ a potential water reservoir in the Earth's interior. Although the actual amount of water constrained from electrical conductivity differ by more than one order of magnitude (Huang et al. 2005; Kelbert et al. 2009; Karato 2011), the discoveries of a hydrous ringwoodite inclusion with ~1.4 wt% water and ice-VII inclusions in natural 'superdeep' diamonds (Pearson et al. 2014; Tschauner et al. 2018) reveal that the MTZ is at least locally hydrated. The presence of water was proposed to narrow the width of the wadsleyite-ringwoodite binary loop (Inoue et al. 2010a), and wadsleyite was found to contain more water than the coexisting ringwoodite with a partition coefficient of 1.6-2.2 at 1673 K (Inoue et al. 2010b). However, available data are not sufficient to quantify the water effect on the phase boundary and the water partition coefficient along the mantle geotherm. It is still unknown how water partitioning between wadsleyite and ringwoodite affects the velocity and density jumps across this phase boundary.

In this study, we used first-principles calculations to investigate the water effect on the wadsleyite-ringwoodite phase transition and the water partition coefficient across this phase boundary. Combining with high P-T elastic data from previous studies (Núñez Valdez et al. 2012; Núñez-Valdez et al. 2013; Wang et al. 2019), we also estimated the velocity and density jumps caused by the wadsleyite-ringwoodite transition under different conditions. This work provides reliable results to infer the nature of the 520-km discontinuity.

2. Methods

2.1 H_2O partition coefficient

The equilibrium partition coefficient of a dilute component between two pure solids is determined by the Gibbs free energies of their pure and dilute phases. Following the procedures in Hernández et al. (2013) and Townsend et al. (2016), the

Gibbs free energy (G) of wadsleyite/ringwoodite with variable water content can be estimated from the Gibbs free energies of pure wadsleyite/ringwoodite (Mg_2SiO_4) and the defective cell containing a single defect. Given a collection of N unit cells of wadsleyite, and n_{Wads} unit cells of wadsleyite which contains a single defect, the Gibbs free energy of this H_2O-bearing wadsleyite can be written as:

$$G_{Wads}(n_{Wads}) = (N - n_{Wads})G_{Wads}^{pure} + n_{Wads}G_{Wads}^{defect} - TS_{Wads}^{conf}(n_{Wads}) \quad (1)$$

where G_{Wads}^{pure} and G_{Wads}^{defect} are the Gibbs free energies of pure wadsleyite (Mg_2SiO_4) and the hydrous wadsleyite with a single defect, respectively. T is temperature, and S_{Wads}^{conf} is configurational entropy, which can be expressed as:

$$S_{Wads}^{conf}(n_{Wads}) = k_B \ln\left(\frac{N_{Wads}!}{(N_{Wads}-n_{Wads})!n_{Wads}!}\right) \quad (2)$$

where N_{Wads} is the number of possible crystallographic sites of the defect in wadsleyite with N unit cells and k_B is the Boltzmann constant. The partial molar derivative of $G_{Wads}(n_{Wads})$ is:

$$\frac{\partial G_{Wads}(n_{Wads})}{\partial n_{Wads}} = -G_{Wads}^{pure} + G_{Wads}^{defect} - T\frac{\partial S_{Wads}^{conf}(n_{Wads})}{\partial n_{Wads}} = G_{Wads}^{f} - T\frac{\partial S_{Wads}^{conf}(n_{Wads})}{\partial n_{Wads}} \quad (3)$$

$$G_{Wads}^{f} = G_{Wads}^{defect} - G_{Wads}^{pure} \quad (4)$$

The partial molar derivative of the configurational entropy is:

$$\frac{\partial S_{Wads}^{conf}(n_{Wads})}{\partial n_{Wads}} = k_B \ln\left(\frac{N_{Wads}-n_{Wads}}{n_{Wads}}\right) \quad (5)$$

Similarly, the partial molar derivative of the Gibbs free energy of hydrous ringwoodite can be written as:

$$\frac{\partial G_{Rw}(n_{Rw})}{\partial n_{Rw}} = -G_{Rw}^{pure} + G_{Rw}^{defect} - T\frac{\partial S_{Rw}^{conf}(n_{Rw})}{\partial n_{Rw}} = G_{Rw}^{f} - T\frac{\partial S_{Rw}^{conf}(n_{Rw})}{\partial n_{Rw}} \quad (6)$$

$$G_{Rw}^{f} = G_{Rw}^{defect} - G_{Rw}^{pure} \quad (7)$$

where G_{Rw}^{pure} and G_{Rw}^{defect} are the Gibbs free energies of pure ringwoodite (Mg_2SiO_4) and the hydrous ringwoodite with a single defect, respectively. $S_{Rw}^{conf}(n_{Rw})$ is configurational entropy and n_{Rw} is the number of unit cells of ringwoodite that

contains a single defect. As such, the partial molar derivative of $S_{Rw}^{conf}(n_{Rw})$ is:

$$\frac{\partial S_{Rw}^{conf}(n_{Rw})}{\partial n_{Rw}} = k_B \ln\left(\frac{N_{Rw}-n_{Rw}}{n_{Rw}}\right) \quad (8)$$

where N_{Wads} is the number of possible crystallographic sites of the defect in ringwoodite. At equilibrium, $\frac{\partial G_{Wads}(n_{Wads})}{\partial n_{Wads}} = \frac{\partial G_{Rw}(n_{Rw})}{\partial n_{Rw}}$, and the H_2O partition coefficient between wadsleyite and ringwoodite ($D_{H2O}^{Wads-Rw}$) is the ratio of the number of defects in wadsleyite and ringwoodite, which can be expressed as:

$$D_{H2O}^{Wads-Rw} = \frac{n_{Wads}}{n_{Rw}} = \frac{N_{Wads}}{N_{Rw}} \frac{e^{\frac{G_{Rw}^f}{k_BT}}+1}{e^{\frac{G_{Wads}^f}{k_BT}}+1} \approx \frac{N_{Wads}}{N_{Rw}} e^{\frac{G_{Rw}^f - G_{Wads}^f}{k_BT}} \quad (9)$$

2.2 Defect structures of hydrous wadsleyite and ringwoodite

The orthorhombic structure of dry wadsleyite with space group *Imma* has three types of Mg sites [M1(4a), M2(4e) and M3(8g)] and four types of O sites [O1(4e), O2(4e), O3(8h) and O4(16j)]. The O1 oxygen, which is not bonded to silicon, is an ideal candidate site for hydroxyls (Smyth 1987). By replacing one M3 Mg atom in the unit cell of wadsleyite ($Mg_{16}Si_8O_{32}$) with two H atoms, we constructed the initial structure of hydrous wadsleyite containing 1.63 wt.% water ($Mg_{15}Si_8O_{30}(OH)_2$). According to previous first-principles calculations (Tsuchiya and Tsuchiya 2009; Wang et al. 2019), the structure with two OH dipoles oriented along the edges of Mg M3 site is most stable (Fig. 1).

Dry ringwoodite ($^{IV}A^{VI}B_2O_4$) has a normal spinel structure with space group Fd-3m. In Mg end-member ringwoodite, the four-coordinated A site (8a) is occupied by Si atom, and the six-coordinated B site (16d) is occupied by Mg atom. Hydrogen was found to be dissolved into ringwoodite through three candidate mechanisms (Panero 2010): (1) V_{Mg}'' +2H**, Mg vacancy with charge-balanced by two H atoms; (2) V_{Si}'''' +4H****, Si vacancy with charge-balanced by four H atoms; (3) Mg_{Si}'' +2H**, Si vacancy is occupied by Mg atom with charge-balanced by two H atoms. Previous first-principles calculations (Panero 2010; Hernández et al. 2013) found that hydrogen is mainly incorporated into ringwoodite through the mechanism V_{Mg}'' +2H**, which is

also supported by the recent experimental results from nuclear resonance spectroscopy (Grüninger et al. 2017). Thus, we adopted the substitution mechanism V_{Mg}'' +2H** to construct the initial structure of hydrous ringwoodite with 1.63 wt% water ($Mg_{15}Si_8O_{30}(OH)_2$), where the sites for two H atoms were determined by following the experimental results from pulsed neutron diffraction (Purevjav et al. 2014) (Fig. 1).

We did not consider the other two mechanisms because they represent different bulk compositions and hence it is difficult to directly compare their energies with that of wadsleyite, which dissolves water via the mechanism V_{Mg}'' +2H**. Because the other two mechanisms have relatively higher formation enthalpies than the mechanism V_{Mg}'' +2H** (Panero 2010), it can be inferred that hydrous ringwoodite would have higher energy when all three possible mechanisms are taken into account. Based on the relative defect energies and the ratios between different mechanisms ((1):(2):(3)= 65:25:10) calculated in Panero (2010), the energy will increase by 3-5 kJ/mol at 1000-1500 K. Thus, the phase-transition pressure will correspondingly increase by 0.6-1.0 GPa and the water partition coefficient between wadsleyite and ringwoodite will increase by 0.2-0.4. It should be noted that these values are only the first-order estimates for the effect of the other two mechanisms.

2.3 First-principles calculations

Calculating the Gibbs free energies of anhydrous and hydrous wadsleyite and ringwoodite is key to obtain the water partition coefficient between these two phases. In theory, the Gibbs free energy G at given pressure P and temperature T is defined by:

$$G(P,T) = F(V,T) + PV \quad (10)$$

where $F(V,T)$ is the Helmholtz free energy at certain volume V and temperature T. Within the quasi-harmonic approximation (QHA), the F can be expressed in as:

$$F(V,T) = U(V) + \frac{1}{2}\sum_{q,m}\hbar\omega_{q,m}(V) + k_BT\sum_{q,m} ln\{1 - exp[-\frac{\hbar\omega_{q,m}(V)}{k_BT}]\} \quad (11)$$

In Eq. (11), $q, m, \omega_{q,m}$ are the phonon wave vector, the normal index, and vibrational frequencies of the system respectively; $\hbar$ and k_B refer to the Planck and Boltzmann constants, respectively; the first, second, third terms are the static internal, zero-point,

and vibrational energy contributions under temperature T at equilibrium volume V, respectively.

To obtain the static internal energies and vibrational density of states at variable volumes, we performed first-principles calculations using Quantum Espresso package (Giannozzi et al. 2009) based on the density functional theory (DFT), adopting the generalized gradient approximation (GGA) (Perdew et al. 1996) for the exchange-correlation functional. The pseudopotential for magnesium was generated by the von Barth and Car method and pseudopotentials for silicon and oxygen were generated by Troullier-Martins method (Troullier and Martins 1991). More relevant details about the generations for Mg, Si, and O pseudopotentials can be found in Tsuchiya et al. (2004). The pseudopotential for hydrogen is PBE type generated by Troullier-Martins method with the valence configuration of $1s^1$ and the cutoff radius of 1.1 Bohr. Electronic wave functions were expanded by a plane-wave basis with an energy cutoff of 70 Ry. All structures were well optimized at different pressures using the variable cell-shape damped molecular dynamics approach (Wentzcovitch 1991) on a 6×6×6 q-point mesh and then their vibrational frequencies were calculated using the ab initio lattice dynamics (LD) (Alfè 2009). Thus, the Helmholtz free energies were calculated from the static energies and vibrational density of states (Eq. (11)) based on the QHA. The calculated Helmholtz free energy versus volume was fitted by the isothermal third-order finite strain equation of state. Thermodynamic properties including pressures at variable volumes and temperatures (equation of state) can be calculated from $F(V,T)$ and the Gibbs free energy can be obtained using Eq. (10). The volume versus pressure relationship is described by the Birch-Murnaghan third-order equation of state.

3. Results

3.1 Relaxed structures of hydrous wadsleyite and ringwoodite

The crystal structures of hydrous wadsleyite and ringwoodite containing 1.63 wt.% H_2O via the substitution mechanism $Mg^{2+} \leftrightarrow 2H^+$ are shown in Fig. 1. The hydrogen

bond lengths for all the defect structures ($Mg_{15}Si_8O_{30}(OH)_2$) at different pressures are given in Table 1. At ambient pressure, the calculated H–O bond at static conditions for hydrous wadsleyite is 0.992 Å, close to the experimental data (Purevjav et al. 2016). Over the entire pressure range investigated in this study (0–25 GPa), the H–O bonds for the defect structures of hydrous ringwoodite are relatively longer than those for hydrous wadsleyite. As a consequence, hydrous wadsleyite has a stronger H–O bond and a higher vibrational frequency for the H–O bond compared to hydrous ringwoodite. This can be well explained by the difference in oxygen for H–O bonds. In wadsleyite, H atoms are bonded to the O1 atoms that are not bonded to silicon (Smyth 1987), while all oxygen atoms in ringwoodite are bonded to both Mg and Si atoms. Upon compression from 0 to 20 GPa, the H–O bond in hydrous wadsleyite lengthens by ~1.0%, and in hydrous ringwoodite, the H–O bond lengthens by ~2.7%. As shown in Table 1, the hydrogen bonds in hydrous wadsleyite and ringwoodite are highly asymmetric and non-linear. The hydrogen bond in hydrous ringwoodite is much stronger, with a hydrogen bond length d(H...O) about 18% shorter than in hydrous wadsleyite. Meanwhile, the hydrogen-bonded oxygen distance d(O...O) in hydrous ringwoodite is also about 12% shorter than in hydrous wadsleyite. At 0-20 GPa, both d(H...O) and d(O...O) significantly decrease with pressure, with a decrease of 10-12% in d(H...O) and 5-8% in d(O...O).

3.2 Water effect on wadsleyite-ringwoodite phase transition

The phase boundary between wadsleyite and ringwoodite can be obtained by comparing their Gibbs free energies (Fig. 2). Our calculations show that Mg_2SiO_4 undergoes a phase transition from wadsleyite to ringwoodite at 22.7 GPa and 1800 K and the Clapeyron slope is about +3.9 MPa/K (Fig. 3 and 4), consistent with previous GGA calculations (Yu et al. 2008). The transition pressure predicted in this study is about 3 GPa higher than previous experimental measurements (Katsura and Ito 1989; Suzuki et al. 2000; Inoue et al. 2006), but the calculated Clapeyron slope agrees well with experimental results (Fig. 4). Typically, the local density approximation (LDA)

underestimates but GGA overestimates the phase-transition pressures for silicate minerals (Yu et al. 2008). Instead, the calculated Clapeyron slope is not essentially sensitive to the exchange-correlation functional used in DFT calculations (Yu et al. 2008; Wentzcovitch et al. 2010). We also calculated the phase boundary for the $Mg_{15}Si_8O_{32}H_2$ system, as shown in Fig. 3 and 4. The incorporation of $2H^+$ into the Mg site increases the difference of Gibbs free energy between ringwoodite and wadsleyite nearby the phase-transition pressures, shifting the phase boundary to higher pressures. For instance, at 1500 K, the phase-transition pressure increases from 21.6 GPa in $Mg_{16}Si_8O_{32}$ to 22.8 GPa in $Mg_{15}Si_8O_{32}H_2$. The pressure shift decreases with increasing temperature because $Mg_{15}Si_8O_{32}H_2$ ringwoodite has a larger value of configurational entropy than $Mg_{15}Si_8O_{32}H_2$ wadsleyite. Accordingly, the Clapeyron slope decreases from +3.9 MPa/K in $Mg_{16}Si_8O_{32}$ to +2.5 MPa/K in $Mg_{15}Si_8O_{32}H_2$. Here we considered the hydrous wadsleyite/ringwoodite as a simple phase with a single component to approximate the water effect on the phase boundary. The presence of water in the $Mg_{16}Si_8O_{32}$ system, more accurately, will result in the coexistence of wadsleyite and ringwoodite at a certain pressure range.

In order to determine the two-phase coexistence domain of the Mg_2SiO_4-H_2O system, we calculated the Gibbs free energies of wadsleyite and ringwoodite as a function of water concentration using Eq. (1-2), as shown in Fig. 5. For instance, at 1500 K and 20 GPa, the Gibbs free energy of wadsleyite is lower than that of ringwoodite (Fig. 5a), suggesting that wadsleyite is a stable phase under the current conditions. At 24 GPa, the Gibbs free energy of ringwoodite is smaller than that of wadsleyite, indicating the completion of the phase transition. At 22 GPa, these two curves cross over, and the wadsleyite-ringwoodite phase transition occurs. At equilibrium, the chemical potentials of the two phases should be equal. Thus, the water concentrations in wadsleyite and ringwoodite can be derived by calculating the common tangent of two crossed curves. Using this approach, we obtained the dependences of water concentrations in wadsleyite and ringwoodite on pressure at

different temperatures (Fig. 5d-5f). The two-phase loop can be determined by searching the two pressures where wadsleyite and ringwoodite have equal water concentrations. Our results show that at the water concentration of 1.0 wt%, wadsleyite and ringwoodite coexist within 0.22 GPa at 1500 K (Fig. 5d), corresponding to 5.5 km. Such a narrow interval will decrease to 0.05 GPa (1.3 km) at 1800 K (Fig. 5e) and less than 0.02 GPa (500 m) at 2000 K (Fig. 5f), suggesting that the presence of water does not significantly change the sharpness of Mg_2SiO_4 wadsleyite-ringwoodite transition. Similarly, previous experimental works also found that the pressure interval is not greater than 0.2 GPa in the Mg_2SiO_4 system (Inoue et al. 2010a). By comparison, the pressure interval of two-phase coexistence for the $(Mg_{0.9}Fe_{0.1})_2SiO_4$ system is about 1.0 GPa at 1873 K (Akaogi et al. 1989; Katsura and Ito 1989; Tsujino et al. 2019).

Here the Gibbs free energies of wadsleyite and ringwoodite were calculated based on the QHA, which assumes temperature-independent phonon frequencies. With increasing temperature, the anharmonic effect will become significant and may need to be considered. However, the anharmonic contribution declines with increasing pressure, and previous studies have verified the validity of QHA at MTZ conditions (Yu et al. 2008; Wentzcovitch et al. 2010). We also did not consider the combined effects of iron and water on the two-phase loop because huge computation is required to quantify the Gibbs free energies of wadsleyite and ringwoodite as a function of iron and water concentrations. The pressure interval for a hydrous and Fe-bearing system can be inferred from the slopes of lower- and upper-boundary pressures on water concentration (k_{wads} and k_{rw}). As shown in Fig. 6, the pressure interval at a water concentration of x will be $\Delta P = (P_{rw}-P_{wads})-x*(k_{wads}- k_{rw})$, where $P_{rw}-P_{wads}$ is the pressure interval under dry condition. For the $(Mg_{0.9}Fe_{0.1})_2SiO_4$ system with 1.0 w% H_2O, Inoue et al. (2010a) suggested that compared to the anhydrous boundary, the lower and upper boundaries at 1673 K shift towards the higher pressure by 0.6-0.8 GPa and ~0.2 GPa, respectively, corresponding to a k_{wads} of 0.6-0.8 GPa/wt% and a k_{rw} of 0.2 GPa/wt%. Thus, ΔP for the $(Mg_{0.9}Fe_{0.1})_2SiO_4$ system with 1.0 w% H_2O is 0.2-0.4 GPa (5-10 km). Notably,

because the pressure interval for the Fe-bearing system under dry conditions decreases with temperature (Tsujino et al. 2019), ΔP is < 0.24 GPa (6 km) under the representative temperature of mid-MTZ (~1800 K), if k_{wad} and k_{rw} at 1673 K are used. Therefore, we conclude that for the $(Mg_{0.9}Fe_{0.1})_2SiO_4$ system, the incorporation of 1.0 wt% water can narrow the effective width of two-phase coexistence by two-thirds.

3.3 H_2O partition coefficient between wadsleyite and ringwoodite

From the Gibbs free energy differences between anhydrous and hydrous phases, we computed the H_2O partition coefficient between wadsleyite and ringwoodite ($D^{Wads\text{-}Rw}_{H2O}$) in Fig. 7. The $D^{Wads\text{-}Rw}_{H2O}$ is larger than one at every P-T point along the phase boundary, indicating that there are more Mg-2H defects in wadsleyite than ringwoodite in thermodynamic equilibrium. Along the phase boundary, the $D^{Wads\text{-}Rw}_{H2O}$ decreases from ~3.2 at 1000 K to ~1.1 at 2000 K, indicating that more water is preferentially incorporated into wadsleyite relative to the coexisting ringwoodite at equilibration. This is consistent with the stronger H-O bonds in wadsleyite than ringwoodite (Table 1) because the O atoms for H-O bonds in wadsleyite are not bonded to silicon (Fig. 1) (Smyth 1987). Experimental works found that the ratio of H_2O in wadsleyite to coexisting ringwoodite is ~1.5 at 1673 K (Chang et al. 2015), consistent with our results (Fig. 7a), although the GGA overestimates the phase boundary by ~3 GPa. (Inoue et al. 2010b) reported a systematically larger value of 1.6-2.2 for $D^{Wads\text{-}Rw}_{H2O}$ of 1.6-2.2 at 1673 K, likely because we did not consider the effect of Si vacancy in hydrous ringwoodite and there may be uncertainties for the measurements of water concentration (Chang et al. 2015). The comparison of $D^{Wads\text{-}Rw}_{H2O}$ between this work and previous experiments of Fe-bearing system indicates that $D^{Wads\text{-}Rw}_{H2O}$ could not be significantly affected by the presence of iron, probably because wadsleyite and ringwoodite have sufficient Mg sites to accommodate both iron and hydrogen atoms even under water-saturated conditions.

4. Implication for the 520-km discontinuity

Seismic studies have observed a seismic discontinuity around 520 km depth in some regions such as Northeastern China and central Asia (Shearer 1990; Gossler and Kind 1996; Deuss and Woodhouse 2001; Tian et al. 2016), but it is be absent in other regions such as the northeastern Pacific Ocean (Gossler and Kind 1996; Deuss and Woodhouse 2001). Beyond that, instead of one 520-km discontinuity, seismic studies have also found two discontinuities at ~500 km and 560 km depths in some regions (Deuss and Woodhouse 2001), which are ascribed to the wadsleyite-ringwoodite phase transition and the exsolution of Ca-perovskite from garnet (Saikia et al. 2008), respectively.

Our results show that the width of the wadsleyite-ringwoodite phase loop in the Mg_2SiO_4-H_2O system is < 1.3 km at 1800 K, while the incorporation of 1.0 wt% water in the $(Mg_{0.9}Fe_{0.1})_2SiO_4$ system can narrow the effective width of this binary phase loop to ~6 km (Inoue et al. 2010a). Such a depth interval is much thinner than the one under dry conditions (~20 km) and comparable to that of olivine-wadsleyite transition (Katsura et al. 2004). Meanwhile, we also calculated the velocity and density jumps across the wadsleyite-ringwoodite transition under mid-MTZ conditions using the high P-T elastic data from previous studies (Núñez Valdez et al. 2012; Núñez-Valdez et al. 2013; Wang et al. 2019, 2020). We consider two end-member cases, the anhydrous system, and wadsleyite with 1.0 wt% H_2O. The water content of ringwoodite is determined by the H_2O partition coefficient (~1.3) in this study. For the $(Mg_{0.9}Fe_{0.1})_2SiO_4$ system, the iron partition coefficient (~0.6) from previous experiments (Inoue et al. 2010a, 2010b) is used to determine the Fe contents in wadsleyite and ringwoodite. Our results show for the $(Mg_{0.9}Fe_{0.1})_2SiO_4$ system, ΔV_P and ΔV_S are ~2.3%, corresponding to V_P and V_S increases of 1.3% in a width of 20 km for a pyrolitic composition. Such small velocity gradients may not be sufficient to produce resolvable seismic signals for a discontinuity at ~520 km. Compared to the anhydrous condition, the presence of 1.0 wt% water will slightly decrease ΔV_P and ΔV_S but increase $\Delta\rho$, which jointly results in a mild increase (~0.2%) in impedance contrasts

($\Delta(\rho V_P)$ and $\Delta(\rho V_S)$) (Table 2). Together with the water effect on the width of the binary phase loop, we conclude that the presence of water in the MTZ will cause much steeper velocity gradients across the wadsleyite-ringwoodite transition, which could promote the occurrence of the 520-km discontinuity. Although this interpretation does not affect the observations using low-frequency seismic methods such as SS precursors and ScS reverberations, the presence of water significantly improves the detectability of the 520-km discontinuity using receiver function methods.

Tian et al. (2016) detected a discontinuity around 520 km in the MTZ as well as deeper 410-km and 660-km discontinuities beneath Northeastern China, where the stagnant Pacific slab was also found by tomographic studies (Zhao 2004b, 2004a; Zhao and Tian 2013). The presence of water in the regional MTZ likely plays a profound role in the detectability of the 520-km discontinuity. A clear low-velocity anomaly above 410 km in this area also indicates a locally hydrous MTZ (Zhao et al. 2009), which may be caused by the water released from the Pacific slab dehydration. Meanwhile, the presence of water in the MTZ can help to explain the depression of the 410-km and 660-km discontinuities in this region. Because the Clapeyron slope is positive for the olivine-wadsleyite transition but is negative for the post-spinel transition (Bina and Helffrich 1994; Helffrich and Wood 2001; Higo et al. 2001; Hirose 2002; Fei et al. 2004; Katsura et al. 2004), the deeper 410-km and 660-km discontinuities cannot be merely explained by a thermal anomaly. The presence of water will uplift the 410-km discontinuity but deepen the 660-km discontinuity (Higo et al. 2001; Chen et al. 2002; Smyth and Frost 2002). As a result, the coupling effect of water and temperature anomaly can provide a good explanation for the simultaneous depression of the 410-km and 660-km discontinuities.

The accurate depth of the 520-km discontinuity could vary in a wide depth range because the phase boundary between wadsleyite and ringwoodite is likely affected by multiple factors such as water, temperature, and oxidation conditions (Mrosko et al. 2015). For instance, the presence of 1.0 wt% water will deepen the 520-km

discontinuity by ~8 km at 1800 K (Fig. 4 and 5), while the lower-temperature anomaly will cause an uplift. The hydration effect on the depth of the 520-km discontinuity is slightly stronger but weaker than these on the 660-km and 410-km discontinuity (Higo et al. 2001; Chen et al. 2002), respectively. However, the 520-km discontinuity is more sensitive to temperature changes than the 410-km and 660-km discontinuities because the Clapeyron slope of the wadsleyite-ringwoodite transition (~+3.9 MPa/K, Fig. 4) is much larger than those of the olivine-wadsleyite and post-spinel transitions (Bina and Helffrich 1994; Helffrich and Wood 2001; Higo et al. 2001; Hirose 2002; Fei et al. 2004; Katsura et al. 2004). This may partly explain the greater depth variation of the 520-km discontinuity than the MTZ bounding discontinuities (Shearer 1990; Gossler and Kind 1996; Deuss and Woodhouse 2001; Tian et al. 2016). Further seismic studies on the 520-km discontinuity could shed more light on the local hydration and thermal states in the MTZ.

5. Conclusion

In this study, we performed first-principles calculations to investigate water partitioning between wadsleyite and ringwoodite and the water effect on the wadsleyite-ringwoodite phase transition. Our results show that upon compression from 0 to 20 GPa, the H–O bond in hydrous wadsleyite lengthens by ~1.0%, and in hydrous ringwoodite, the H–O bond lengthens by ~2.7%. The transition pressure for the Mg_2SiO_4 system predicted in this study is about 3 GPa higher than previous experimental measurements (Katsura and Ito 1989; Suzuki et al. 2000; Inoue et al. 2006), but the calculated Clapeyron slope agrees well with experimental results. The incorporation of $2H^+$ into the Mg site increases the difference of Gibbs free energy between ringwoodite and wadsleyite nearby the phase-transition pressures, shifting the phase boundary to higher pressures. At the water concentration of 1.0 wt%, wadsleyite and ringwoodite coexist within 0.05 GPa (1.3 km) at 1800 K, suggesting that the presence of water does not significantly change the sharpness of Mg_2SiO_4 wadsleyite-ringwoodite transition. For

the $(Mg_{0.9}Fe_{0.1})_2SiO_4$ system with 1.0 w% H_2O, the pressure interval is 0.2-0.4 GPa (5-10 km), which is much smaller than that under dry conditions (~20 km). Along the phase boundary, the H_2O partition coefficient between wadsleyite and ringwoodite decreases from ~3.2 at 1000 K to ~1.1 at 2000 K, indicating that more water is preferentially incorporated into wadsleyite relative to the coexisting ringwoodite at equilibration. Combining high P-T elastic data from previous studies and the H_2O partition coefficient in this study, we find that the presence of 1.0 wt% water will slightly decrease ΔV_P and ΔV_S but increase $\Delta\rho$. Given that the incorporation of 1.0 wt% water can narrow the effective width of two-phase coexistence by two-thirds for the $(Mg_{0.9}Fe_{0.1})_2SiO_4$ system, we suggest that the presence of water in the MTZ will cause much steeper velocity gradients across the wadsleyite-ringwoodite transition, which could promote the occurrence of the 520-km discontinuity.

Acknowledgments

This study is supported by the Natural Science Foundation of China (41925017, 41721002) and the Fundamental Research Funds for the Central Universities (WK2080000144). W.Z. Wang acknowledges support from the UCL-Carnegie Postdoctoral Scholarship. The calculations were conducted partly at the supercomputing center of University of Science and Technology of China.

References

Akaogi, M., Ito, E., and Navrotsky, A. (1989) Olivine-modified spinel-spinel transitions in the system Mg_2SiO_4-Fe_2SiO_4 : Calorimetric measurements, thermochemical calculation, and geophysical application. Journal of Geophysical Research: Solid Earth, 94, 15671–15685.

Alfè, D. (2009) PHON: A program to calculate phonons using the small displacement method. Computer Physics Communications, 180, 2622–2633.

Bina, C.R., and Helffrich, G. (1994) Phase transition Clapeyron slopes and transition zone seismic discontinuity topography. Journal of Geophysical Research, 99, 15853.

Brown, J.M., and Shankland, T.J. (1981) Thermodynamic parameters in the Earth as determined from seismic profiles. Geophysical Journal International, 66, 579–596.

Chang, Y.Y., Jacobsen, S.D., Bina, C.R., Thomas, S.M., Smyth, J.R., Frost, D.J., Boffa Ballaran, T., McCammon, C.A., Hauri, E.H., Inoue, T., and others (2015) Comparative compressibility of hydrous wadsleyite and ringwoodite: Effect of H2O and implications for detecting water in the transition zone. Journal of Geophysical Research B: Solid Earth, 120, 8259–8280.

Chen, J., Inoue, T., Yurimoto, H., and Weidner, D.J. (2002) Effect of water on olivine-wadsleyite phase boundary in the $(Mg, Fe)_2SiO_4$ system. Geophysical Research Letters, 29, 22-1-22–4.

Demouchy, S. (2005) Pressure and temperature-dependence of water solubility in Fe-free wadsleyite. American Mineralogist, 90, 1084–1091.

Deuss, A., and Woodhouse, J. (2001) Seismic Observations of Splitting of the Mid-Transition Zone Discontinuity in Earth's Mantle. Science, 294, 354–357.

Duan, L., Wang, W., Wu, Z., and Qian, W. (2019) Thermodynamic and Elastic Properties of Grossular at High Pressures and High Temperatures: A First-Principles Study. Journal of Geophysical Research: Solid Earth, 124, 2019JB017439.

Dziewonski, A.M., and Anderson, D.L. (1981) Preliminary reference Earth model. Physics of the Earth and Planetary Interiors, 25, 297–356.

Fei, H., and Katsura, T. (2020) High water solubility of ringwoodite at mantle transition zone temperature. Earth and Planetary Science Letters, 531, 115987.

Fei, Y., Van Orman, J., Li, J., van Westrenen, W., Sanloup, C., Minarik, W., Hirose, K., Komabayashi, T., Walter, M., and Funakoshi, K. (2004) Experimentally determined postspinel transformation boundary in Mg_2SiO_4 using MgO as an internal pressure standard and its geophysical implications. Journal of Geophysical Research: Solid Earth, 109, 1–8.

Giannozzi, P., Baroni, S., Bonini, N., Calandra, M., Car, R., Cavazzoni, C., Ceresoli, D., Chiarotti, G.L., Cococcioni, M., Dabo, I., and others (2009) QUANTUM ESPRESSO: a modular and open-source software project for quantum simulations of materials. Journal of Physics: Condensed Matter, 21, 395502.

Gossler, J., and Kind, R. (1996) Seismic evidence for very deep roots of continents. Earth and Planetary Science Letters, 138, 1–13.
Grüninger, H., Armstrong, K., Greim, D., Boffa-Ballaran, T., Frost, D.J., and Senker, J. (2017) Hidden Oceans? Unraveling the Structure of Hydrous Defects in the Earth's Deep Interior. Journal of the American Chemical Society, 139, 10499–10505.
Helffrich, G.R., and Wood, B.J. (2001) The Earth's mantle. Nature, 412, 501–507.
Hernández, E.R., Alfè, D., and Brodholt, J. (2013) The incorporation of water into lower-mantle perovskites: A first-principles study. Earth and Planetary Science Letters, 364, 37–43.
Higo, Y., Inoue, T., Irifune, T., and Yurimoto, H. (2001) Effect of water on the spinel-postspinel transformation in Mg_2SiO_4. Geophysical Research Letters, 28, 3505–3508.
Hirose, K. (2002) Phase transitions in pyrolitic mantle around 670-km depth: Implications for upwelling of plumes from the lower mantle. Journal of Geophysical Research: Solid Earth, 107, ECV 3-1-ECV 3-13.
Huang, X., Xu, Y., and Karato, S. (2005) Water content in the transition zone from electrical conductivity of wadsleyite and ringwoodite. Nature, 434, 746–749.
Inoue, T., Irifune, T., Higo, Y., Sanehira, T., Sueda, Y., Yamada, A., Shinmei, T., Yamazaki, D., Ando, J., Funakoshi, K., and others (2006) The phase boundary between wadsleyite and ringwoodite in Mg_2SiO_4 determined by in situ X-ray diffraction. Physics and Chemistry of Minerals, 33, 106–114.
Inoue, T., Ueda, T., Tanimoto, Y., Yamada, A., and Irifune, T. (2010a) The effect of water on the high-pressure phase boundaries in the system Mg_2SiO_4-Fe_2SiO_4. Journal of Physics: Conference Series, 215, 012101.
Inoue, T., Wada, T., Sasaki, R., and Yurimoto, H. (2010b) Water partitioning in the Earth's mantle. Physics of the Earth and Planetary Interiors, 183, 245–251.
Jacobsen, S.D., Demouchy, S., Frost, D.J., Ballaran, T.B., and Kung, J. (2005) A systematic study of OH in hydrous wadsleyite from polarized FTIR spectroscopy and single-crystal X-ray diffraction: Oxygen sites for hydrogen storage in Earth's interior. American Mineralogist, 90, 61–70.
Karato, S. (2011) Water distribution across the mantle transition zone and its implications for global material circulation. Earth and Planetary Science Letters, 301, 413–423.
Katsura, T., and Ito, E. (1989) The system Mg_2SiO_4-Fe_2SiO_4 at high pressures and temperatures: Precise determination of stabilities of olivine, modified spinel, and spinel. Journal of Geophysical Research: Solid Earth, 94, 15663–15670.
Katsura, T., Yamada, H., Nishikawa, O., Song, M., Kubo, A., Shinmei, T., Yokoshi, S., Aizawa, Y., Yoshino, T., Walter, M.J., and others (2004) Olivine-wadsleyite transition in the system $(Mg, Fe)_2SiO_4$. Journal of Geophysical Research: Solid Earth, 109, n/a–n/a.
Kelbert, A., Schultz, A., and Egbert, G. (2009) Global electromagnetic induction

constraints on transition-zone water content variations. Nature, 460, 1003–1006.
Kennett, B.L.N., Engdahl, E.R., and Buland, R. (1995) Constraints on seismic velocities in the Earth from traveltimes. Geophysical Journal International, 122, 108–124.
Mrosko, M., Koch-Müller, M., McCammon, C., Rhede, D., Smyth, J.R., and Wirth, R. (2015) Water, iron, redox environment: effects on the wadsleyite–ringwoodite phase transition. Contributions to Mineralogy and Petrology, 170, 9.
Núñez-Valdez, M., Wu, Z., Yu, Y.G., and Wentzcovitch, R.M. (2013) Thermal elasticity of $(Fe_x, Mg_{1-x})_2SiO_4$ olivine and wadsleyite. Geophysical Research Letters, 40, 290–294.
Núñez Valdez, M., Wu, Z., Yu, Y.G., Revenaugh, J., and Wentzcovitch, R.M. (2012) Thermoelastic properties of ringwoodite $(Fe_x, Mg_{1-x})_2SiO_4$: Its relationship to the 520 km seismic discontinuity. Earth and Planetary Science Letters, 351–352, 115–122.
Ohtani, E. (2015) Hydrous minerals and the storage of water in the deep mantle. Chemical Geology, 418, 6–15.
Panero, W.R. (2010) First principles determination of the structure and elasticity of hydrous ringwoodite. Journal of Geophysical Research, 115, B03203.
Pearson, D.G., Brenker, F.E., Nestola, F., McNeill, J., Nasdala, L., Hutchison, M.T., Matveev, S., Mather, K., Silversmit, G., Schmitz, S., and others (2014) Hydrous mantle transition zone indicated by ringwoodite included within diamond. Nature, 507, 221–224.
Perdew, J.P., Burke, K., and Ernzerhof, M. (1996) Generalized Gradient Approximation Made Simple. Physical Review Letters, 77, 3865–3868.
Purevjav, N., Okuchi, T., Tomioka, N., Abe, J., and Harjo, S. (2014) Hydrogen site analysis of hydrous ringwoodite in mantle transition zone by pulsed neutron diffraction. Geophysical Research Letters, 41, 6718–6724.
Purevjav, N., Okuchi, T., Tomioka, N., Wang, X., and Hoffmann, C. (2016) Quantitative analysis of hydrogen sites and occupancy in deep mantle hydrous wadsleyite using single crystal neutron diffraction. Scientific Reports, 6, 34988.
Ringwood, A.E. (1962) A model for the upper mantle. Journal of Geophysical Research, 67, 857–867.
Saikia, A., Frost, D.J., and Rubie, D.C. (2008) Splitting of the 520-Kilometer Seismic Discontinuity and Chemical Heterogeneity in the Mantle. Science, 319, 1515–1518.
Shearer, P.M. (1990) Seismic imaging of upper-mantle structure with new evidence for a 520-km discontinuity. Nature, 344, 121–126.
Shearer, P.M., and Flanagan, M.P. (1999) Seismic Velocity and Density Jumps Across the 410- and 660-Kilometer Discontinuities. Science, 285, 1545–1548.
Smyth, J.R. (1987) The beta-Mg_2SiO_4: a potential host for water in the mantle? American Mineralogist, 72, 1051–1055.
Smyth, J.R., and Frost, D.J. (2002) The effect of water on the 410-km discontinuity:

532 An experimental study. Geophysical Research Letters, 29, 4.
533 Suzuki, A., Ohtani, E., Morishima, H., Kubo, T., Kanbe, Y., Kondo, T., Okada, T.,
534 Terasaki, H., Kato, T., and Kikegawa, T. (2000) In situ determination of the
535 phase boundary between Wadsleyite and Ringwoodite in Mg_2SiO_4. Geophysical
536 Research Letters, 27, 803–806.
537 Tian, Y., Zhu, H., Zhao, D., Liu, C., Feng, X., Liu, T., and Ma, J. (2016) Mantle
538 transition zone structure beneath the Changbai volcano: Insight into deep slab
539 dehydration and hot upwelling near the 410 km discontinuity. Journal of
540 Geophysical Research: Solid Earth, 121, 5794–5808.
541 Townsend, J.P., Tsuchiya, J., Bina, C.R., and Jacobsen, S.D. (2016) Water
542 partitioning between bridgmanite and postperovskite in the lowermost mantle.
543 Earth and Planetary Science Letters, 454, 20–27.
544 Troullier, N., and Martins, J.L. (1991) Efficient pseudopotentials for plane-wave
545 calculations. II. Operators for fast iterative diagonalization. Physical Review B,
546 43, 8861–8869.
547 Tschauner, O., Huang, S., Greenberg, E., Prakapenka, V.B., Ma, C., Rossman, G.R.,
548 Shen, A.H., Zhang, D., Newville, M., Lanzirotti, A., and others (2018) Ice-VII
549 inclusions in diamonds: Evidence for aqueous fluid in Earth's deep mantle.
550 Science, 359, 1136–1139.
551 Tsuchiya, J., and Tsuchiya, T. (2009) First principles investigation of the structural
552 and elastic properties of hydrous wadsleyite under pressure. Journal of
553 Geophysical Research, 114, B02206.
554 Tsuchiya, T., Tsuchiya, J., Umemoto, K., and Wentzcovitch, R.M. (2004) Phase
555 transition in MgSiO3 perovskite in the earth's lower mantle. Earth and Planetary
556 Science Letters, 224, 241–248.
557 Tsujino, N., Yoshino, T., Yamazaki, D., Sakurai, M., Sun, W., Xu, F., Tange, Y., and
558 Higo, Y. (2019) Phase transition of wadsleyite-ringwoodite in the Mg_2SiO_4-
559 Fe_2SiO_4 system. American Mineralogist, 104, 588–594.
560 Wang, W., Walter, M.J., Peng, Y., Redfern, S., and Wu, Z. (2019) Constraining
561 olivine abundance and water content of the mantle at the 410-km discontinuity
562 from the elasticity of olivine and wadsleyite. Earth and Planetary Science
563 Letters, 519, 1–11.
564 Wang, W., Zhang, H., Brodholt, J.P., and Wu, Z. (2020) Elasticity of hydrous
565 ringwoodite at mantle conditions: Implication for water distribution in the
566 lowermost mantle transition zone. Earth and Planetary Science Letters, 554,
567 116626.
568 Wentzcovitch, R.M. (1991) Invariant molecular-dynamics approach to structural
569 phase transitions. Physical Review B, 44, 2358–2361.
570 Wentzcovitch, R.M., Yu, Y.G., and Wu, Z. (2010) Thermodynamic Properties and
571 Phase Relations in Mantle Minerals Investigated by First Principles
572 Quasiharmonic Theory. Reviews in Mineralogy and Geochemistry, 71, 59–98.
573 Yu, Y.G., Wu, Z., and Wentzcovitch, R.M. (2008) α–β–γ transformations in Mg_2SiO_4

574 in Earth’s transition zone. Earth and Planetary Science Letters, 273, 115–122.
575 Zhao, D. (2004a) Global tomographic images of mantle plumes and subducting slabs:
576 insight into deep Earth dynamics. Physics of the Earth and Planetary Interiors,
577 146, 3–34.
578 Zhao, D. (2004b) Origin of the Changbai intraplate volcanism in Northeast China:
579 Evidence from seismic tomography. Chinese Science Bulletin, 49, 1401.
580 Zhao, D., and Tian, Y. (2013) Changbai intraplate volcanism and deep earthquakes in
581 East Asia: a possible link? Geophysical Journal International, 195, 706–724.
582 Zhao, D., Tian, Y., Lei, J., Liu, L., and Zheng, S. (2009) Seismic image and origin of
583 the Changbai intraplate volcano in East Asia: Role of big mantle wedge above
584 the stagnant Pacific slab. Physics of the Earth and Planetary Interiors, 173, 197–
585 206.
586 Zou, F., Wu, Z., Wang, W., and Wentzcovitch, R.M. (2018) An Extended
587 Semianalytical Approach for Thermoelasticity of Monoclinic Crystals:
588 Application to Diopside. Journal of Geophysical Research: Solid Earth, 123,
589 7629–7643.
590

Table 1. Hydrogen bond geometries at static conditions for hydrous wadsleyite and ringwoodite ($Mg_{15}Si_8O_{30}(OH)_2$) calculated in this study.

Minerals	Pressure (GPa)	d(H-O) (Å)	frequency (cm^{-1})	d(H...O) (Å)	d(O...O) (Å)	
Hydrous wadsleyite	0	0.992	3286	2.014	2.998	This study
	0	1.00	-	-	3.01	ref. 1*
	0	0.999	-	2.089	-	ref. 2†
	0	0.987	-	2.105	-	ref. 2‡
	5	0.995	3227	1.935	2.921	This study
	10	0.997	3172	1.869	2.856	This study
	15	1.000	3121	1.812	2.802	This study
	20	1.002	3072	1.764	2.756	This study
	25	1.004	3022	1.723	2.716	This study
Hydrous ringwoodite	0	1.025	2748	1.668	2.653	This study
	5	1.031	2638	1.620	2.612	This study
	10	1.038	2529	1.576	2.577	This study
	15	1.045	2422	1.539	2.547	This study
	20	1.053	2306	1.500	2.518	This study
	25	1.062	2193	1.465	2.492	This study

ref. 1, Tsuchiya and Tsuchiya (2009); ref. 2, Purevjav et al. (2016). *, static conditions; †, 100 K; ‡, 295 K.

Table 2. Predicted velocity and density contrasts between ringwoodite and wadsleyite at 18 GPa and 1800 K.

Systems	Mg_2SiO_4	Mg_2SiO_4+1.0 wt% H_2O	$(Mg_{0.9}Fe_{0.1})_2SiO_4$	$(Mg_{0.9}Fe_{0.1})_2SiO_4$+1.0 wt% H_2O
Width of binary phase loop (km)	-	~1.3	~20	~6
ΔK_S	7.70%	7.50%	8.45%	8.28%
ΔG	9.04%	8.77%	8.31%	7.99%
$\Delta\rho$	1.96%	2.67%	3.85%	4.54%
ΔV_P	3.15%	2.68%	2.28%	1.81%
ΔV_S	3.54%	3.05%	2.23%	1.72%
$\Delta(\rho V_P)$	5.11%	5.35%	6.12%	6.36%
$\Delta(\rho V_S)$	5.51%	5.72%	6.08%	6.27%

Elasticity of wadsleyite and ringwoodite is available in previous studies (Núñez Valdez et al. 2012; Núñez-Valdez et al. 2013; Wang et al. 2019). The water partition coefficient (~1.3) in this study and the iron partition coefficient (~0.6) from previous experiments is used.

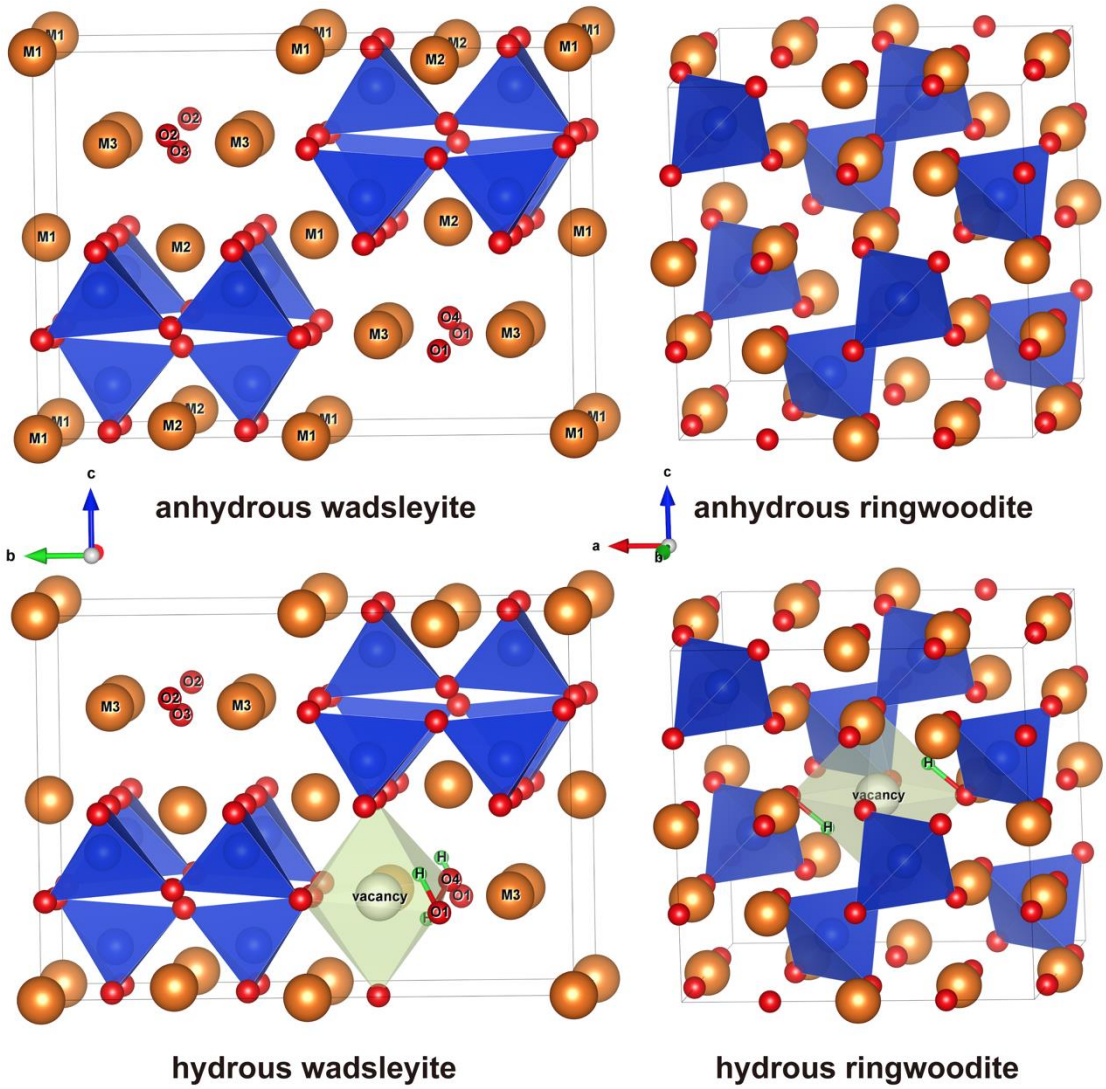

Figure 1. Relaxed crystal structures of anhydrous and hydrous wadsleyite and ringwoodite. In all structures, orange, red, dark blue, and green spheres represent magnesium, oxygen, silicon, and hydrogen atoms, respectively.

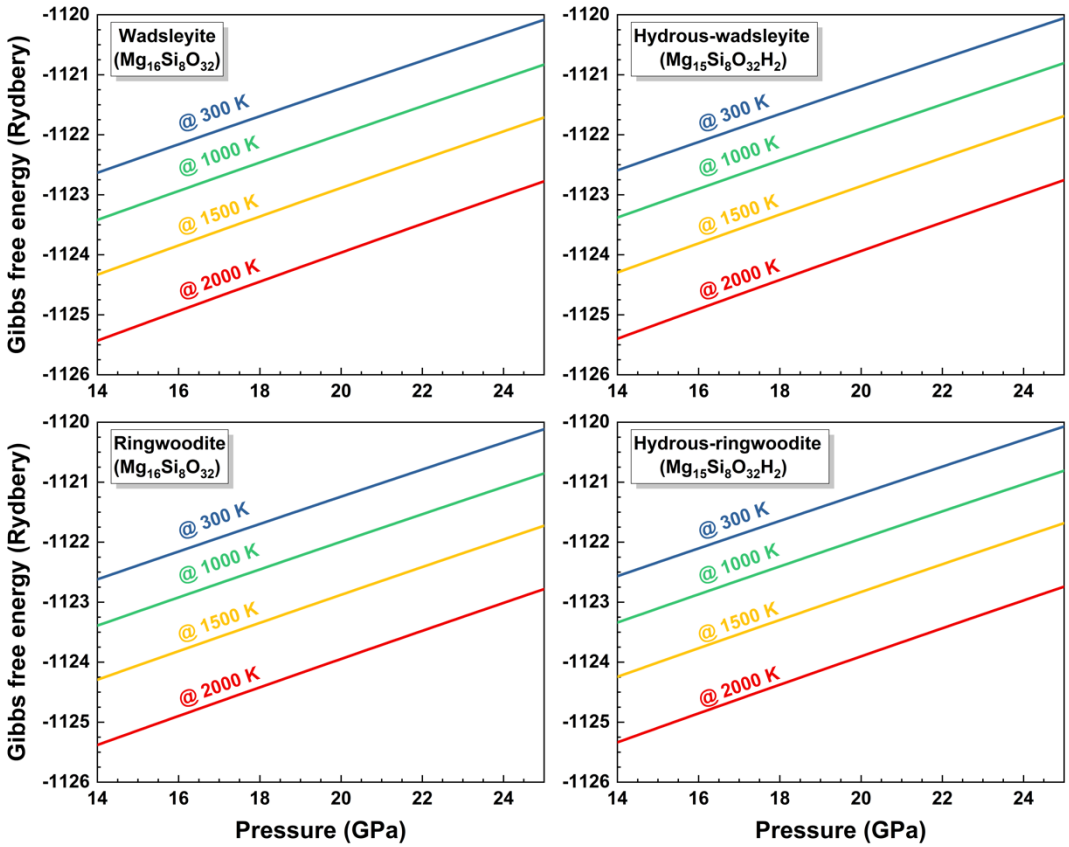

Figure 2. Gibbs free energy of anhydrous and hydrous wadsleyite and ringwoodite ($Mg_{16}Si_8O_{32}$ and $Mg_{15}Si_8O_{32}H_2$) as a function of pressure at various temperatures. The Gibbs free energies of hydrous phases ($Mg_{15}Si_8O_{32}H_2$) do not include the contribution of the configurational entropy.

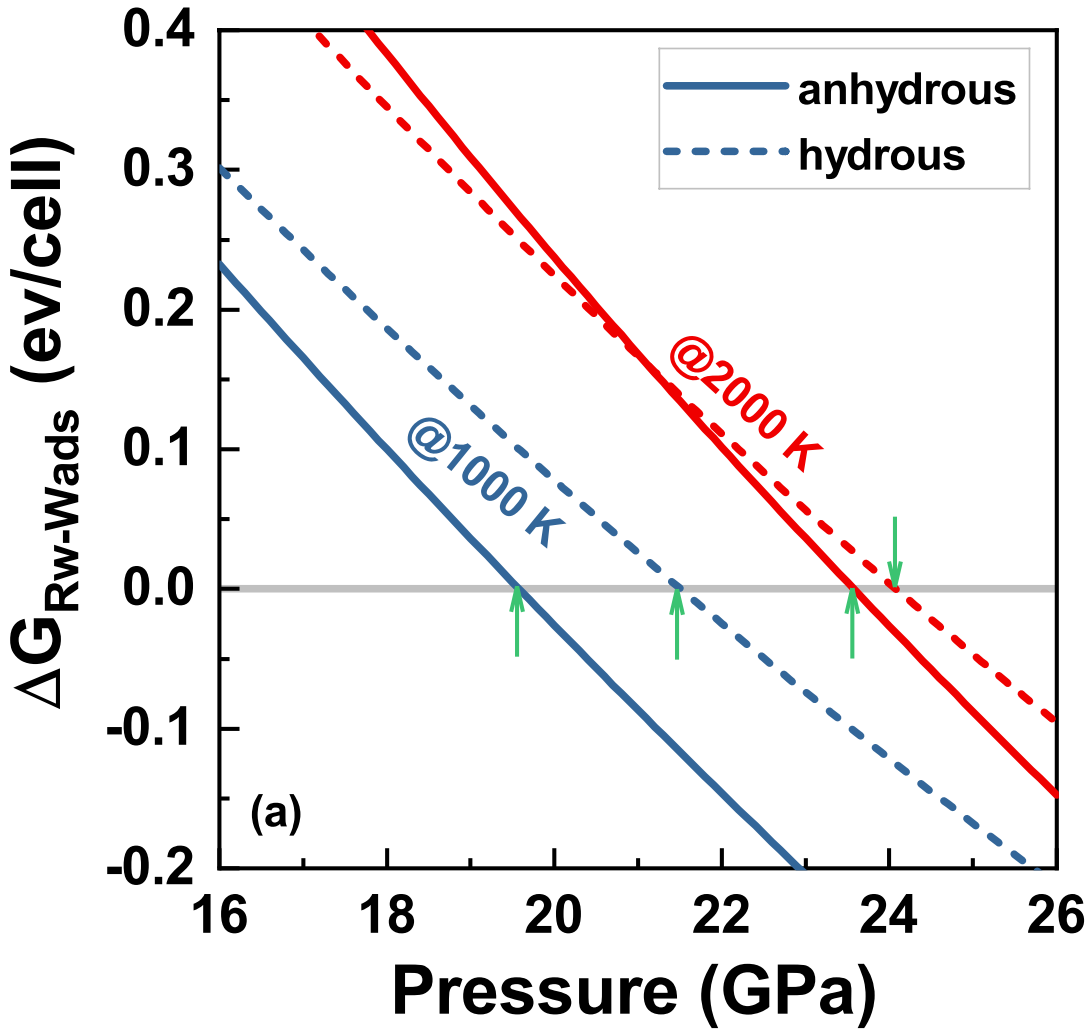

Figure 3. The differences of Gibbs free energy between ringwoodite and wadsleyite. Solid and dash lines represent the G differences between wadsleyite and ringwoodite for $Mg_{16}Si_8O_{32}$ and $Mg_{15}Si_8O_{32}H_2$ systems, respectively. The configurational entropies (Eq. (2)) in hydrous wadsleyite and ringwoodite are included to calculate the ΔG.

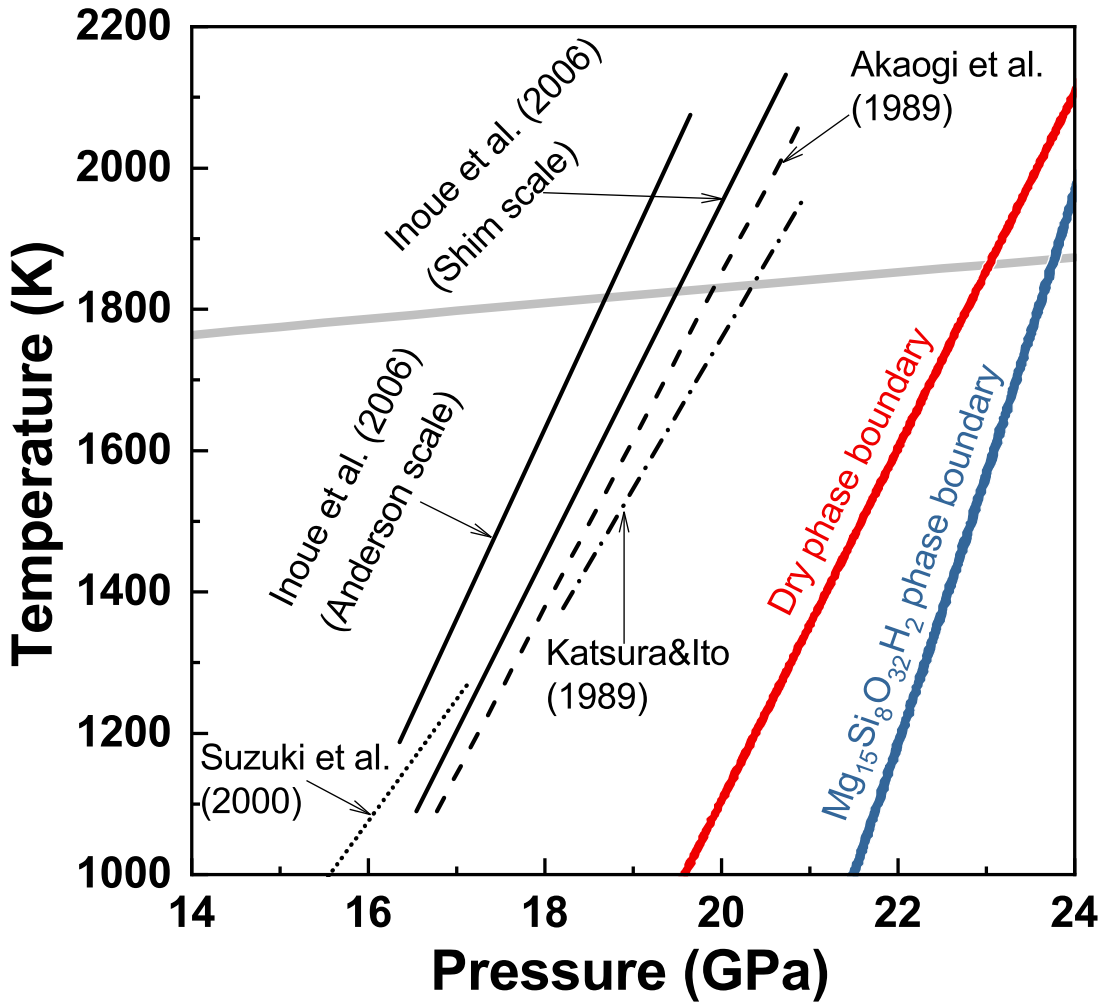

Figure 4. Phase boundary between wadsleyite and ringwoodite. Red and blue lines represent the phase boundaries for $Mg_{16}Si_8O_{32}$ and $Mg_{15}Si_8O_{32}H_2$ systems, respectively. Experimental results: black lines, (Inoue et al. 2006); dash line, Akaogi et al (1989); short dash line, Suzuki et al. (2000); dash dot line, Katsura and Ito (1989). The grey line is the mantle adiabat Brown and Shankland (1981).

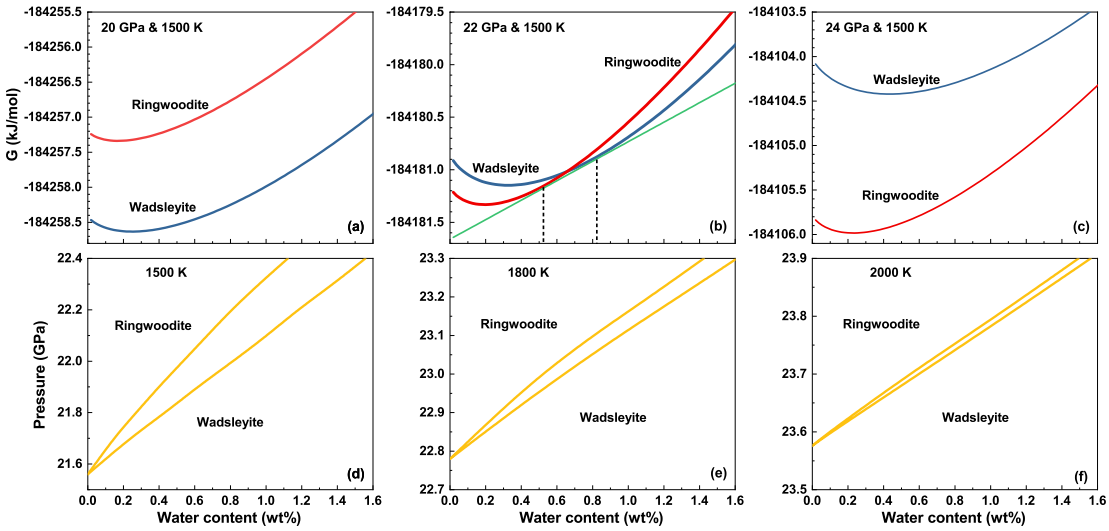

Figure 5. Top: the Gibbs free energies of wadsleyite and ringwoodite versus water concentration at 1500 K and (a) 20 GPa, (b) 22 GPa, (c) 24 GPa. Red and blue lines represent the Gibbs free energies of wadsleyite and ringwoodite, respectively. The green line in (b) is the cotangent line of two crossed curves. Bottom: water effect on the phase loop of wadsleyite-ringwoodite transition in the Mg_2SiO_4-H_2O system at (d) 1500 K, (e) 1800 K, (f) 2000 K. Wadsleyite and ringwoodite coexist within 0.05 GPa or 1.3 km at 1800 K when the water concentration is 1.0 wt%.

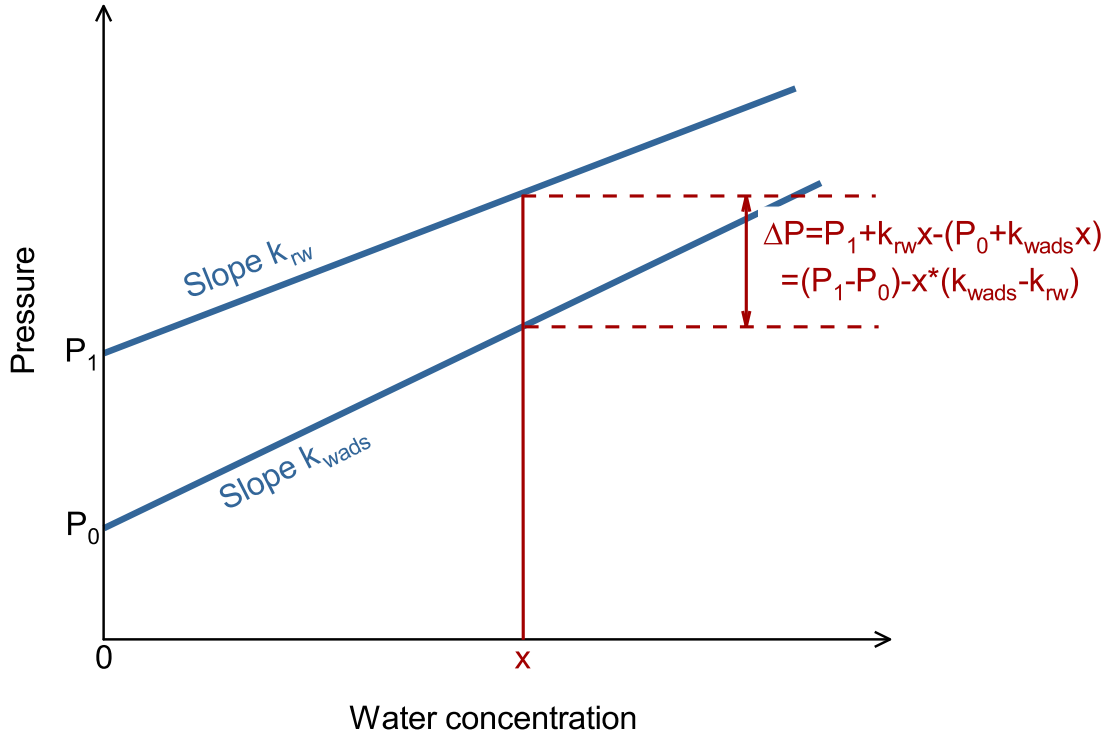

Figure 6. Schematic diagrams of the relationship between the pressure interval of two-phase coexistence for the $(Mg_{0.9}Fe_{0.1})_2SiO_4$-$H_2O$ system. The pressure interval at a water concentration of x is $\Delta P=(D^{Wads\text{-}Rw}_{H2O}-1)*k_{wads}*x$. In the $(Mg_{0.9}Fe_{0.1})_2SiO_4$-$H_2O$ system, the pressure interval is $\Delta P=(P_{rw}-P_{wads})-x*(k_{wads}-k_{rw})$, where is $P_{rw}-P_{wads}$ the pressure interval for the $(Mg_{0.9}Fe_{0.1})_2SiO_4$ system under dry condition. For the $(Mg_{0.9}Fe_{0.1})_2SiO_4$ system with 1.0 w% H_2O, Inoue et al. (2010a) suggested that compared to the anhydrous boundary, the lower and upper boundaries at 1673 K shift towards the higher pressure by 0.6-0.8 GPa and ~0.2 GPa, respectively, corresponding to a k_{wads} of 0.6-0.8 GPa/wt% and a k_{rw} of 0.2 GPa/wt%.

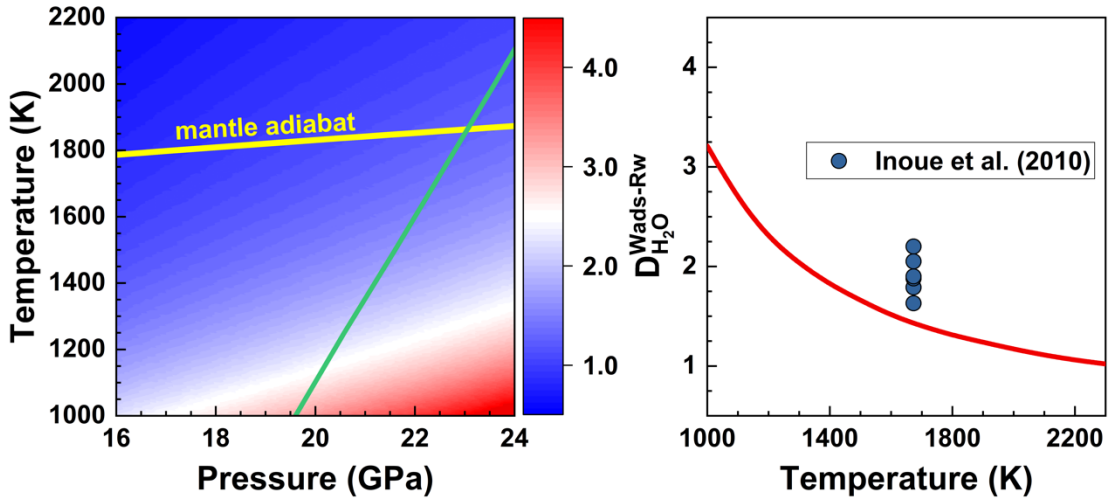

Figure 7. (a) Map of the water partition coefficient between wadsleyite and ringwoodite. The yellow line is the mantle adiabat Brown and Shankland (1981). (b) water partition coefficient along the phase boundary. Experimental results are from Inoue et al. (2010b).